nanomaterials

Article

Anti-reflective coatings produced by atomic layer deposition for hybrid-polymer 3D micro-optics

Darija Astrauskytė [1], Karolis Galvanauskas [2], Darius Gailevičius [2], Mantas Drazdys [1], Mangirdas Malinauskas [2,*] and Lina Grineviciute [1,*]

[1] Center for Physical Sciences and Technology, Savanorių av. 231, LT-02300, Vilnius, Lithuania;
[2] Laser Research Center, Physics Faculty, Vilnius University, Saulėtekio av. 10, LT-10223, Vilnius, Lithuania;
* Correspondence: mangirdas.malinauskas@ff.vu.lt (M.M.), lina.grineviciute@ftmc.lt (L.G.)

Abstract: The increasing demand for optics quality requires the lowest optical power loss, which can occur from unwanted reflections. Laser direct writing (LDW) allows for the fabrication of complex structures, which is particularly advantageous in micro-optic applications. This research demonstrates the possibility of forming an anti-reflective coating on hybrid-polymer micro-lenses fabricated by employing LDW without changing their geometry. Such coating deposited by atomic layer deposition (ALD) decreased the reflection from 3.3 % to 0.1 % at the wavelength of 633 nm for one surface of hybrid organic-inorganic SZ2080™ material. This research validates the compatibility of ALD with LDW 3D multiphoton lithography synergetically, expanding its applications on optical grade sub-100 micrometers scale micro-optics.

Keywords: atomic layer deposition; anti-reflective coating; micro-optics; SZ2080™; multi-photon lithography; direct laser writing

Citation: Astrauskytė, D.; Galvanauskas, K.; Gailevičius, D.; Drazdys, M.; Malinauskas, M.; Grineviciute, L. Anti-reflective coatings produced by atomic layer deposition for hybrid-polymer 3D micro-optics. **2023**, *13*, x. https://doi.org/10.3390/xxxxx

Academic Editor(s):

Received: date
Accepted: date
Published: date

1. Introduction

Anti-reflective (AR) coatings are widely used in various optical applications to reduce unwanted reflections and enhance light transmission efficiency. These coatings are particularly beneficial in optical devices such as lenses, mirrors, and displays, where reflections can cause glare, reduce contrast, and distort the image quality [1]. AR coatings are typically designed to minimize the reflection at a specific wavelength [2], several wavelengths [3], or over a range of wavelengths [4, 5], depending on the application. Physical vapor deposition (PVD) techniques, such as electron beam evaporation, ion beam sputtering, magnetron sputtering etc., are the most widely used methods for fabricating AR coatings, offering numerous advantages, including high deposition rates, good film uniformity, and the deposition of high-quality optical coatings with high laser-induced damage thresholds [6-8]. However, significant progress has been made in designing and fabricating optical components over the past few decades. Multi-photon polymerization enables the fabrication of complex shape micro-optics such as multi-lens micro-objectives [9], micro-lens arrays [10], free-form micro-lenses [10] or stacked gratings [11], which often suffer from reduced efficiency due to reflection losses. For such applications, PVD technologies are becoming insufficient and have limitations [12], such as poor conformality to cover micro and macro free-form optics Fig. 1 (a)). In recent years, atomic layer deposition (ALD) has emerged as a promising alternative to PVD for fabricating coatings on complex shape 3D substrates [5, 13-16]. ALD is a modified chemical vapor deposition (CVD) technique that allows precise film thickness control at the atomic level by sequentially exposing the substrate to alternating gaseous precursors. The process involves self-limiting surface reactions, where each precursor molecule reacts with the available reactive site of the substrate surface, forming a single atomic layer [17]. This makes it possible to achieve uniform and conformal coatings on complex substrates (Fig. 1 (a)).

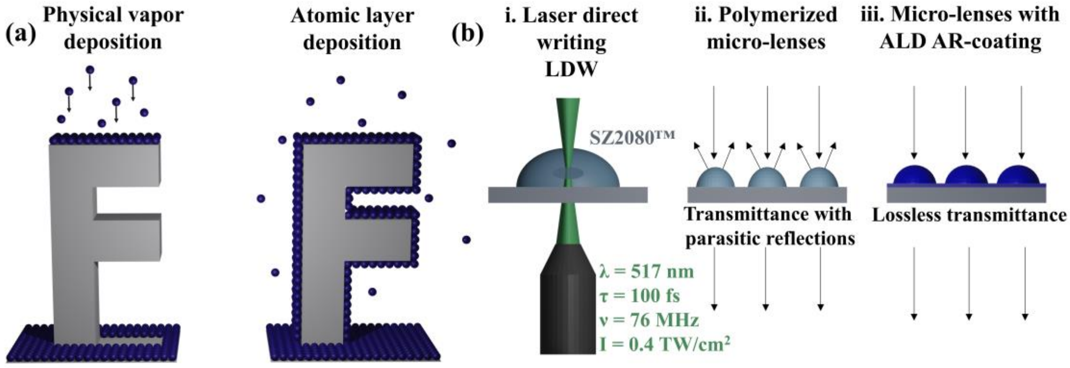

Figure 1. (**a**) The schematic representation of differences between physical vapor deposition and atomic layer deposition on the complex substrate; (**b**) Fabrication of highly transparent micro-optics combining laser direct writing and atomic layer deposition.

This study aims to demonstrate the ability to deposit AR coatings by ALD on micro-lenses with sizes less than 100 μm (Fig. 1 (b)). The feasibility of the method is performed using SZ2080™ which is compatible with the heat-treatment post-processing [18] offering high optical damage resilience [19].

2. Materials and Methods

The hybrid organic-inorganic polymer SZ2080™ was selected for fabricating the 3D microstructures due to its favorable characteristics, including high optical transmittance and the ability to adjust the refractive index [20, 21]. However, it is important to determine the dispersions of the refractive index and optical losses of SZ2080™ to model the design of the AR coating, as SZ2080™ is not widely used as a substrate for optical coatings. To investigate the growth dynamics of alumina on SZ2080™, the polymer was drop-casted on a quartz crystal sensor. Before the deposition of the AR coating, it was necessary to evaluate the optical properties of the hybrid polymer SZ2080™; therefore, the polymer was spin-coated on fused silica (FS) substrate to form a layer of a few microns. Optical characteristics of SZ2080™ were determined from transmittance spectra using OptiChar [22] software and used in the design of the AR coating. Finally, the influence of the ALD deposited coating on the micro-lenses geometry and optical function was studied.

2.1. Preparation of spin-coated samples

To confirm the feasibility of ALD AR coating on LDW-fabricated microstructures from hybrid organic-inorganic polymer SZ2080™, polymer film properties were investigated. Such films are usually produced using UV curing while employing an appropriate photoinitiator (PI) [20]. During the film production, it was important to avoid adding any photoinitiator, which would introduce time-dependent additional variability [23]. Therefore, we choose to perform thermal curing that tends to produce consistent degrees of crosslinking [24]. For SZ2080™ this approach is based on the spontaneous thermal polymerization of the methacrylic groups [25] and the heat-catalyzed condensation reaction of the inorganic network [20].

First, SZ2080™ was spin-coated on FS substrates using Chemat Technology spin coater (9 s 600 RPM, 30 s 2000 RPM) and heat-cured at 120 °C for 2 hours. Control samples were immersed in the developer methyl-isobutyl-ketone for 10 minutes to indirectly confirm the saturation of the crosslinking reaction. After annealing, the film thickness, refractive index and optical losses of the SZ2080™ layer were evaluated from the transmittance spectra.

SZ2080™ was also drop-casted onto the Inficon 750-1058-G10 quartz crystal sensor and then dried at 50 °C for 12 hours. The lower temperature was chosen to allow for slow solvent evaporation without forming entrapped bubbles. Before quartz crystal microbalance (QCM) measurements, a prepared sample was placed in the ALD reactor and exposed to 20 sccm N_2 flow for 12 hours to stabilize the oscillations of the quartz crystal sensor.

2.2. Fabrication of 3D microstructures

In this work, microstructures and micro-lenses were fabricated by ultrafast 3D nanolithography done by direct laser writing. Microstructures were polymerized utilizing a laser oscillator with 517 nm wavelength, 100 fs pulse duration and 76 MHz repetition rate. Scanning was done with *Femtika NanoFactory* [26] system, utilizing Aerotech IFOV technology known as continuous 3D writing [27]. Fabrication power was set to ≈ 3 mW, resulting in ≈ 0.5 TW/cm^2 intensity; scanning speed - 1 mm/s. 3D models of the microstructures were made using *OpenSCAD* [28]. At the same time, fabrication machine code was generated using *3DPoli* [26] software. Two models of lenses were used - with diameters of 50 µm and 100 µm and focal lengths of 140-190 µm (Fig. 2 (a)). The final diameter and height of polymerized lenses depend on the fabrication's initial Z-stage position, which is set manually (fig. 2 (b)). Flat structures - square and circular platforms (with dimensions of 50 µm × 50 µm × 5 µm) - were also fabricated and coated. Methyl-isobutyl-ketone was used as a solvent to remove unpolymerized resist. Fabricated microstructures are depicted in Figure 2 (c). Note that SZ2080™ hybrid material was used pure without the PI addition, as the femtosecond pulses can induce photopolymerization reactions directly via multiple excitation mechanisms, as revealed recently [29].

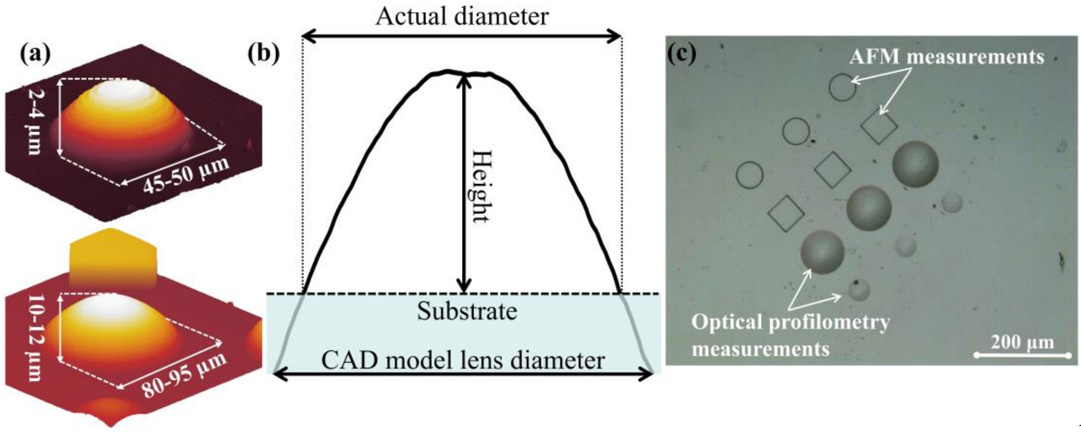

Figure 2. (**a**) 3D profiles of the fabricated ≈ 50 µm and ≈ 100 µm diameter micro-lenses; (**b**) Comparison between modelled and fabricated micro-lens diameter; (**c**) Optical micrograph of the 3D microstructures and micro-lenses fabricated using direct laser writing. These microstructures were used for depositions of thin films.

2.3. Deposition of thin films

Thin film deposition was performed using Veeco Savannah S200 ALD system equipped with a capacitively coupled plasma generator. The depositions were carried out at 60 °C; 25.4 mm diameter FS substrates were used as substrates to deposit titania and alumina thin films. Tetrakisdimethylaminotitanium (TDMAT) was used as a Ti-containing precursor, trimethylaluminum (TMA) was used as an Al source. Oxygen plasma was used as an oxidizer. Argon was used as a carrier gas at a flow of 40 sccm. For plasma generation, a 100 sccm flow of oxygen was used. All deposition parameters are summarized in Table 1.

Table 1. Optimized parameters for deposition of Al_2O_3 and TiO_2.

Material	Precursor pulse duration, s	Purge duration, s	O_2 plasma pulse duration, s	Purge duration, s	Plasma power, W
TiO_2	0.15	15	6	15	200
Al_2O_3	0.02	8	6	8	100

2.4. Characterization methods

Al_2O_3 thin film growth on SZ2080™ was monitored using *in situ* QCM. The quartz crystal sensor was positioned in the center of the ALD reactor. Transmittance and reflectance spectra were measured by Photon RT Spectrophotometer in the spectral range from 185 nm to 2000 nm. Film thickness, refractive index and optical losses of the thin films were determined from transmittance spectra using OptiChar software.

The stress in the thin films was calculated using Stoney formula [30]. Interferometry was used to characterize the curvature radius of the substrates before and after the deposition of the thin films. Optical profilometry was used to measure the profile of the micro-lenses before and after the deposition of different coatings (Fig. 2 (c)). Atomic force microscopy (AFM) was used to evaluate the surface roughness of the microstructures before and after the deposition of different coatings (Fig. 2 (c)).

The focal lengths of the micro-lenses were evaluated using an optical microscope by imaging a square aperture and USAF 1951 resolution target. The imaging object was positioned on the microscope condenser diaphragm, essentially providing a virtual object at a distance significantly greater than the focal length of the micro-lens, and the image plane was adjusted until it was in focus. By placing the object at a distance much greater than the focal length, it could be assumed that the object is located at infinity and that the image being viewed is in the focal plane.

The relative transmittance of the micro-lenses was approximately determined by utilizing a square aperture as the object (Figure 3). An image of the aperture was captured using a filter that closely matched the AR coating spectrum. The CCD sensor operated in grayscale mode, and a fixed portion of the square image was integrated to obtain a numerical average of the gray color. No gamma correction or additional post-processing was applied, assuming that the obtained image brightness is linearly proportional to the amount of light transmitted. However, it is important to note that this method is only suitable for comparing elements of identical shape, as it provides relative transmittance values.

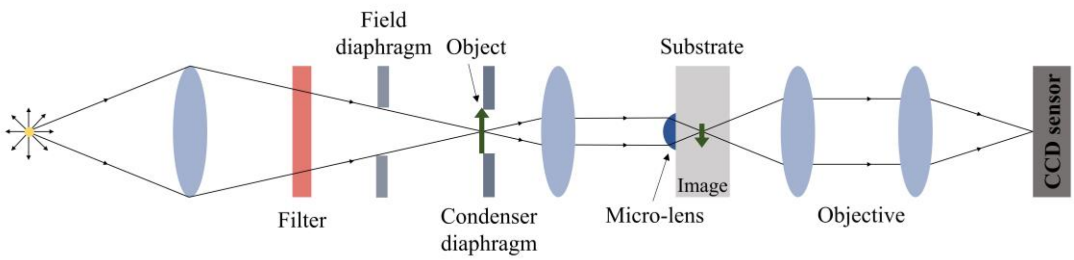

Figure 3. Optical system scheme for micro-lens image detection.

3. Results and discussion

3.1. Growth dynamics of aluminum oxide on SZ2080™

The growth dynamics of thin films strongly depend on the substrate, with the most significant differences occurring at the beginning of the film growth. The initial nucleation period plays a crucial role in producing continuous ultrathin films that could be utilized in the design of optical coatings [31]. Alumina growth dynamics on different polymers have been extensively studied [32-34], but to date, there has been no investigation conducted on hybrid organic-inorganic polymers such as SZ2080™. In this study, the growth dynamics of Al_2O_3 by ALD on drop-casted hybrid polymer SZ2080™ were investigated using *in situ* QCM at 150 °C. Figure 4 (a) shows aluminum oxide growth dynamics on SZ2080™ (black line). For demonstration purposes, growth dynamics on bare quartz crystal coated with Au are also shown (red line). At the first 50 cycles of aluminum oxide growth on quartz crystal, the growth rate is initially low due to a lack of nucleation sites, resulting in island-like growth, as described by R. L. Puurunen and W. Vandervorst [35]. In the case of SZ2080™, in the first two cycles growth rate is initially high before rapidly decreasing and then increasing until reaching linear growth (Fig. 4 (b)). This behavior can be attributed to the porous surface of the hybrid polymer [36]. Linear growth started after the eight cycles when continuous Al_2O_3 film was formed.

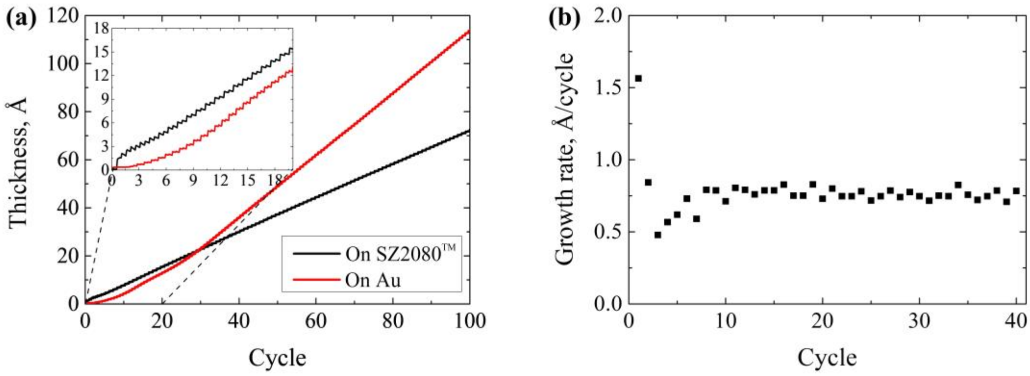

Figure 4. (**a**) Al_2O_3 film thickness as a function of the number of atomic layer deposition cycles measured by quartz crystal microbalance. The inset shows data collected in the first 20 cycles; (**b**) The growth rate of the Al_2O_3 as a function of the number of cycles measured by quartz crystal microbalance.

3.2. Spin-coated and thermally polymerized SZ2080™ film optical characteristics

Before the deposition of optical coatings, the optical properties of the spin-coated SZ2080™ film were characterized. The thickness of the SZ2080™ film was approximately 2 μm. Figure 5 (a) shows the transmittance spectrum of the spin-coated SZ2080™ layer. Using this spectrum, the refractive index and optical losses of the SZ2080™ were simulated (Fig. 5 (b)). At the wavelength of 633 nm refractive index of the spin-coated SZ2080™ film is 1,48. Compared to the literature, a lower degree of cross-linking without the use of the PI achieved via thermal polymerization can result in a lower refractive index [20, 21, 37].

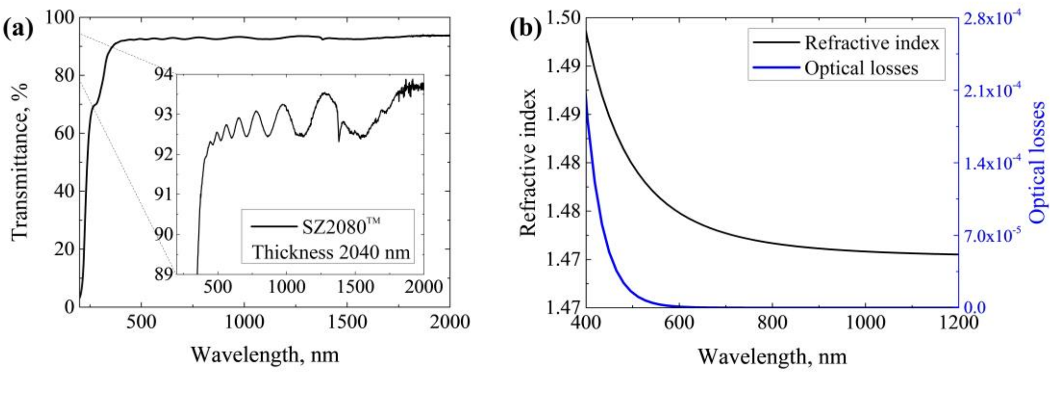

Figure 5. (**a**) Transmittance spectrum of spin-coated ≈ 2 μm thick SZ2080™ layer; (**b**) Dispersions of refractive index and optical losses of spin-coated SZ2080™ layer.

3.3. Single-layer coatings

Alumina and titania were deposited on FS substrates to characterize the thin film's optical properties, which will be used in the design of AR coating. Figure 6 (a) shows the transmittance spectra of Al_2O_3 and TiO_2 thin films with thicknesses of around 300 nm, while (b) shows the dispersion curves of the refractive indices and optical losses. Refractive indices of TiO_2 and Al_2O_3 at the wavelength of 633 nm are 2.38 and 1.61, respectively. Obtained optical properties of titania and alumina thin films are comparable with the previously reported study where the same precursors were used [38].

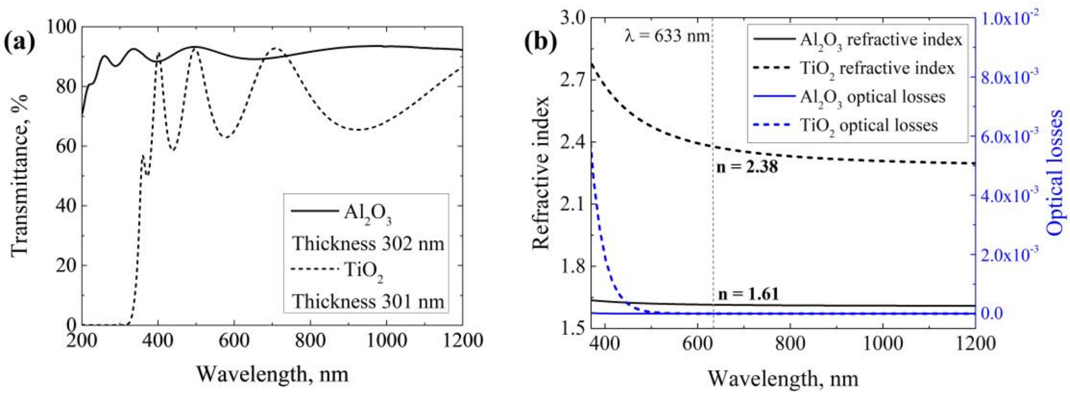

Figure 6. (**a**) Transmittance spectra of ≈ 300 nm thick Al_2O_3 and TiO_2 thin films; (**b**) Dispersions of refractive index and optical losses of Al_2O_3 and TiO_2 thin films.

After the characterization of optical properties, physical characteristics were analyzed. The surface roughness of microstructures was evaluated by AFM. Figure 7 depicts 3D AFM images of microstructures before and after the deposition of aluminum and titanium oxides. After the deposition of Al_2O_3 and TiO_2 thin films, the surface roughness of the microstructures slightly decreased (see the explanation provided in subsection 3.4).

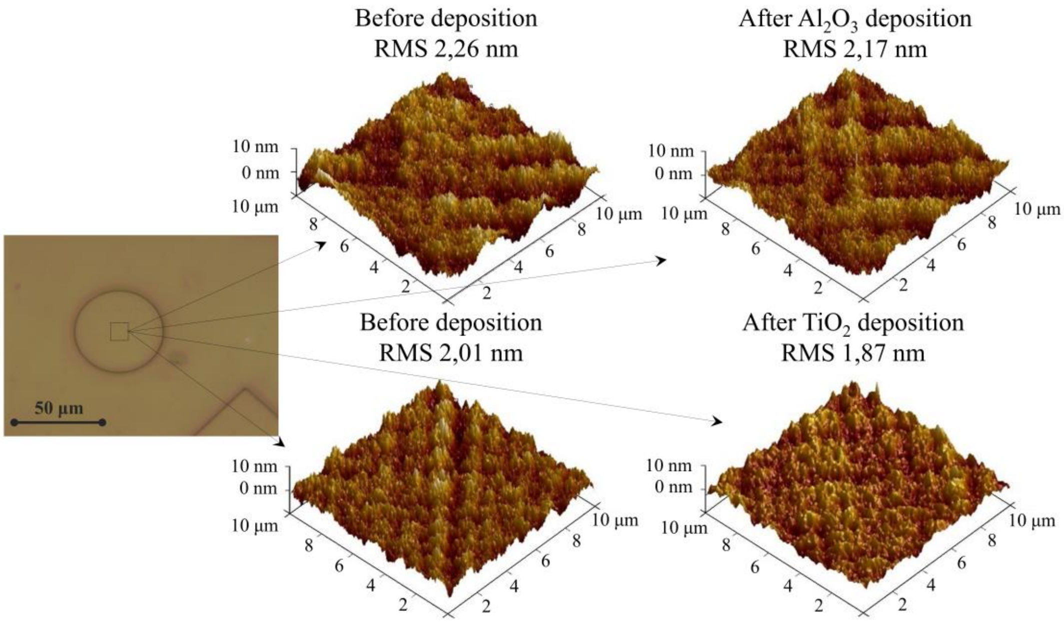

Figure 7. 3D atomic force microscope images of microstructures' morphology before and after the deposition of Al_2O_3 and TiO_2 films (scan area 10 µm × 10 µm).

Optical profilometry was used to determine the profiles of the micro-lenses. Figure 8 displays profiles of the ≈ 50 µm and ≈ 80 µm diameter micro-lenses before and after the deposition of different single-layer coatings ((a) Al_2O_3, (b) TiO_2). The focal lengths of three ≈ 50 µm diameter and three ≈ 80 µm diameter micro-lenses were measured before (f_0) and after the deposition (f) of thin films, and the averaged values are presented in Table 2, which also includes the averaged changes in the micro-lenses' focal length (Δf) after the depositions and stress values of the thin films. As can be seen, changes in the micro-lens focal lengths correlate with changes in the micro-lens height. In the case of aluminum oxide, focal length decreases by 7.5-8 % while the height of the micro-lenses increases. A different effect is observed after the deposition of TiO_2 - focal length increases by 2-7 % and the height of the lenses decreases. Al_2O_3 and TiO_2 thin films were determined to be under tensile stress within the values 135 MPa and 86 MPa, respectively. The relationship between the stress of the alumina coating and the changes in the micro-lens geometry is not clear. It can be assumed that the growth of the thin film influenced these changes. TMA molecules are initially smaller compared to TDMAT; consequently, these molecules can penetrate into porous polymer media, inducing an increase in the micro-lens height. Conversely, TDMAT molecules are significantly larger and cannot diffuse into the polymer. The observed decrease of micro-lens height after the deposition of titania coating is caused by the tensile stress of the thin film.

Table 2 The stress of the single-layer coatings, the focal length of the micro-lenses before deposition (f_0) and after the deposition (f) and coating-induced change in the micro-lens focal length (Δf).

Coating	Stress, MPa	Lens diameter, µm	f_0, µm	f, µm	Δf, %
Al_2O_3	135	50	187 ± 7	172 ± 2	-8 ± 2
		90	184 ± 6	170 ± 9	-7.5 ± 3
TiO_2	86	45	142 ± 4	152 ± 5	7 ± 4
		80	156 ± 3	159 ± 5	2 ± 1

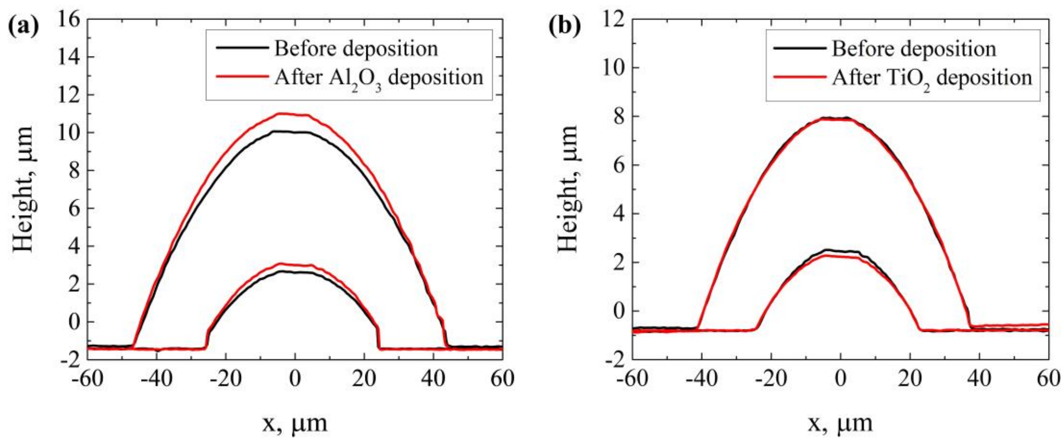

Figure 8. Profiles of the ≈ 50 µm and ≈ 80 µm diameter micro-lenses before and after the deposition of ≈ 300 nm thick (**a**) Al_2O_3; (**b**) TiO_2 film.

3.4. Anti-reflective coating

As the optical properties of the substrate and individual layers were established, the design of anti-reflective coating was simulated using TFCalc [39] (Fig. 9 red curve). The AR coating was fabricated according to the theoretical model and consisted of 23 nm titanium oxide and 130.8 nm aluminum oxide layers. After the deposition, the reflectance of the experimental coating was measured (black line) in the spectral region 200-950 nm. Discrepancies between the theoretical design and experimental curve in the UV range can be attributed to the absorption of TiO_2. Compared to the theoretical transmittance minimum, AR coating reduced the reflectance of one SZ2080™ surface from 3.3 % to 0.1 % at the wavelength of 633 nm.

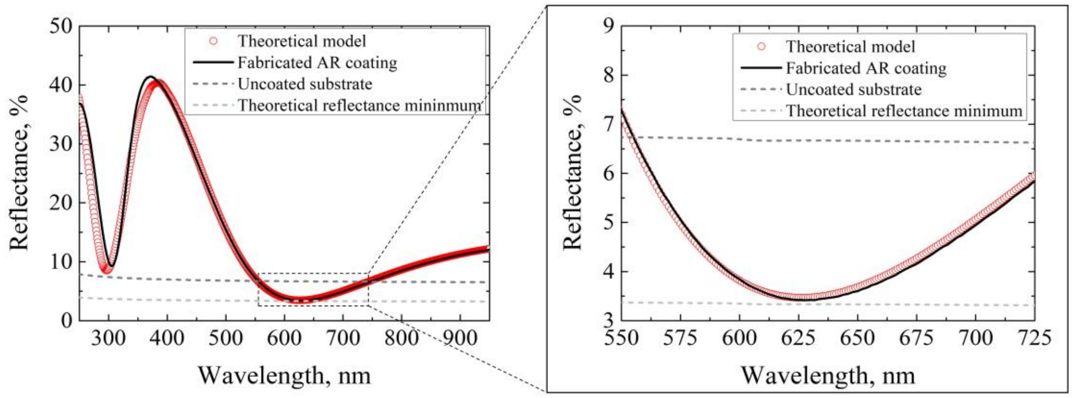

Figure 9. Simulated and experimental reflectance spectra of anti-reflective coating for λ = 633 nm.

The same deposition process of AR coating was applied to micro-lenses, but due to their small size, direct measurement of absolute transmittance was problematic. To overcome this, the relative transmittance of the ≈ 95 μm diameter micro-lenses was evaluated at a wavelength of 633 nm. The measurements were performed on three separate micro-lenses and the averaged values are shown in Figure 10 (a). As can be seen, the relative transmittance of the micro-lenses increased by 3.7 %. In addition, the transmittance of flat surface microstructures was measured and similar results were obtained with a 3.6 % increase in absolute transmittance after AR coating deposition. Also, imaging quality comparison utilizing USAF 1951 target was carried out on the micro-lenses and the images before and after the deposition of AR coating are shown in Figure 10 (b) and (c), respectively. No changes in image quality were observed after the deposition of AR coating.

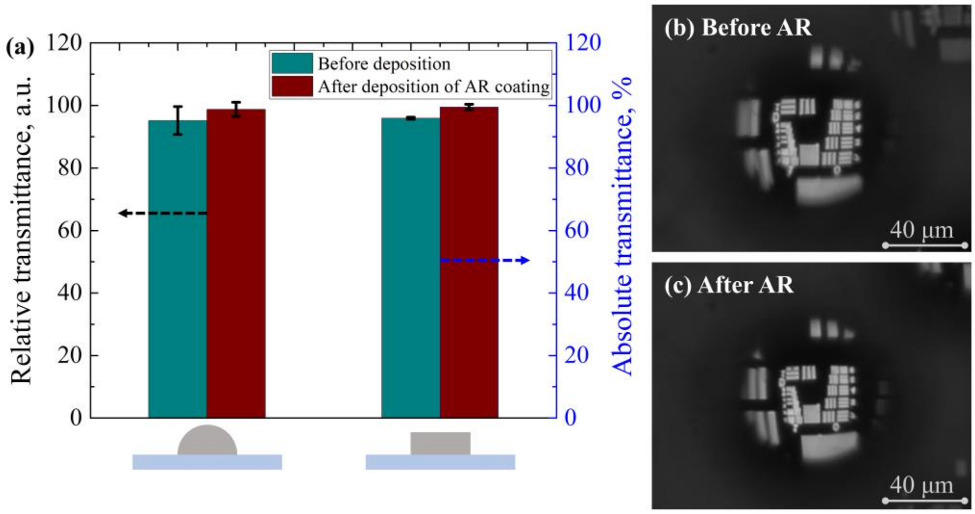

Figure 10. (**a**) Relative transmittance of the ≈ 95 μm micro-lens and absolute transmittance of the flat surface microstructure before and after the deposition of anti-reflective coating at the wavelength of 633 nm; USAF image (**b**) before and (**c**) after anti-reflective coating deposition.

The surface morphology of the microstructures was measured before and after the deposition of the AR coating. As shown in Fig. 11 (a) and (b), AR coating reduced surface roughness from 3.4 nm to 2.6 nm. The observed decrease in surface roughness can be attributed to the ability of the ALD coating to fill in the surface grooves and irregularities, resulting in a smoother substrate surface. Multiple studies [40-42] have also reported that ALD coating smoothens the surface.

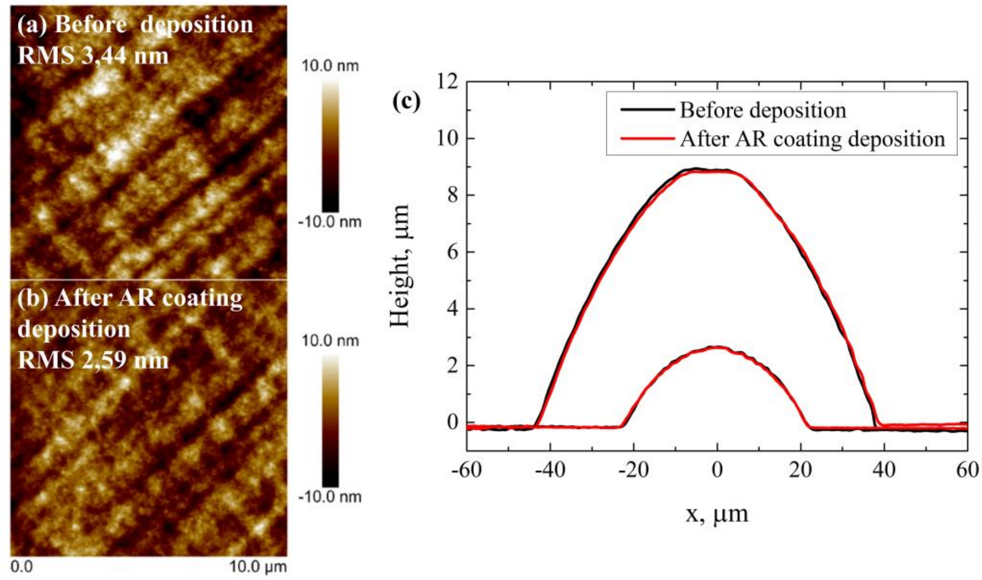

Figure 11. Atomic force microscope top-view images of 3D microstructures surface (**a**) before deposition and (**b**) after deposition of anti-reflective coating (scan area 10 µm × 10 µm); (**c**) Profiles of the ≈ 45 µm and ≈ 95 µm diameter micro-lenses before and after the deposition of anti-reflective coating.

Further, the focal lengths and profiles of the micro-lenses were evaluated before and after the deposition of AR coating. Optical profilometry measurements showed no difference in the micro-lens height after the deposition (Fig. 11 (c)). The focal length measurements were performed using an identical procedure described in subsection 3.3. As can be seen from Table 3, AR coating increases focal length by 1.5-3 %. Stress in the AR coating was found to be tensile, with a value of 127 MPa. The first layer of the AR coating was TiO_2 and a small increase in focal length of the micro-lens was observed after the deposition due to stress of the AR coating.

Table 3. The stress of the anti-reflective coating, the focal length of the micro-lenses before deposition (f_0) and after the deposition (f) and coating-induced change in the micro-lens focal length (Δf).

Coating	Stress, MPa	Lens diameter, µm	f_0, µm	f, µm	Δf, %
AR coating	127	45	182 ± 7	185 ± 6	1.5 ± 0.8
		95	190 ± 5	196 ± 5	3 ± 0.5

The stress of the optical coatings changes the curvature of the flat substrate [43, 44]. In this study, a similar tendency was observed that the stress of the AR coating affects the geometry of the micro-lenses. This knowledge is important for the design of the final element.

4. Conclusions

A quantitative study was performed on the deposition of anti-reflective coating on hybrid polymer microstructures using the atomic layer deposition technique. First, the optical characteristics of the spin-coated and thermally polymerized SZ2080™ film were evaluated. Then, the influence of titania and alumina thin films on micro-lens geometry was analyzed. The findings showed that the focal length of the micro-lenses decreases by 7.5 % - 8 % after Al_2O_3 deposition and increases by 2 % - 7 % after TiO_2 deposition. This suggests that for precision applications primary lens geometry needs to be accommodated to the expected geometry change after applying the coating.

Furthermore, the anti-reflective coating deposited by atomic layer deposition decreased the reflection from 3.3 % to 0.1 % at the wavelength of 633 nm for one surface of SZ2080™. Fabricated anti-reflective coating improved the transmittance of the micro-lens by 3.7 % without significantly affecting their geometry. The results also indicate that the top-layer surface roughness of the microstructures was slightly reduced after all the depositions. The findings prove the feasibility of ALD coatings on laser 3D lithography-made micro-optics with sub-100 micrometer dimensions employing hybrid organic-inorganic photonic materials.

Author Contributions: K.G., D.G. and M.M. fabricated microstructures by LDW and measured the transmittance of microstructures; D.A., M.D. and L.G. carried out the ALD depositions and characterization of thin films; supervised the research. All authors contributed to interpreting the results and preparing the article.

Funding: This work was supported by PerFIN project from the Research Council of Lithuania (LMTLT), agreement No. S-MIP-22-80. K.G., D.G. and M.M. received funding from EU Horizon 2020, Research and Innovation program LASERLAB-EUROPE JRA Project No. 871124.

Data Availability Statement: The data that support the findings of this study are available within the open access article. Additional data can be provided by a request to corresponding authors.

Acknowledgments: We acknowledge Maria Farsari and Vasileia Melissinaki for kindly providing the authors with the SZ2080™ (IESL-FORTH, Heraklion, Greece) hybrid organic-inorganic materials for performing the described experiments.

Conflicts of Interest: The authors declare no conflict of interest.

References

1. Raut, H.K.; Ganesh, V.A.; Nair, A.S.; Ramakrishna, S. Anti-Reflective Coatings: A Critical, in-Depth Review. *Energy Environ. Sci.* **2011**, *4*, 3779, doi:10.1039/c1ee01297e.
2. Wang, Z.; Wang, Y.; He, H.; Shen, Z.; Sytchkova, A.; Chen, R.; Zhang, Y.; Li, D.; Hu, G.; Zheng, Y.; et al. Laser-Induced Damage of 1064 Nm Multilayer Antireflection Coatings after Exposure to Gamma Rays. *Optical Materials* **2021**, *122*, 111580, doi:10.1016/j.optmat.2021.111580.
3. Abromavičius, G.; Buzelis, R.; Drazdys, R.; Juškevičius, K.; Kičas, S.; Tolenis, T.; Mirauskas, J.; Ščiuka, M.; Sirutkaitis, V.; Melninkaitis, A. Optical Resistance and Spectral Properties of Anti-Reflective Coatings Deposited on LBO Crystals by Ion Beam Sputtering. *Lith. J. Phys.* **2011**, *51*, 303–308, doi:10.3952/lithjphys.51407.
4. Xi, J.-Q.; Schubert, M.F.; Kim, J.K.; Schubert, E.F.; Chen, M.; Lin, S.-Y.; Liu, W.; Smart, J.A. Optical Thin-Film Materials with Low Refractive Index for Broadband Elimination of Fresnel Reflection. *Nature Photon* **2007**, *1*, 176–179, doi:10.1038/nphoton.2007.26.
5. Pfeiffer, K.; Ghazaryan, L.; Schulz, U.; Szeghalmi, A. Wide-Angle Broadband Antireflection Coatings Prepared by Atomic Layer Deposition. *ACS Appl. Mater. Interfaces* **2019**, *11*, 21887–21894, doi:10.1021/acsami.9b03125.
6. Tolenis, T.; Grinevičiūtė, L.; Buzelis, R.; Smalakys, L.; Pupka, E.; Melnikas, S.; Selskis, A.; Drazdys, R.; Melninkaitis, A. Sculptured Anti-Reflection Coatings for High Power Lasers. *Opt. Mater. Express* **2017**, *7*, 1249, doi:10.1364/OME.7.001249.
7. Vlček, J.; Belosludtsev, A.; Rezek, J.; Houška, J.; Čapek, J.; Čerstvý, R.; Haviar, S. High-Rate Reactive High-Power Impulse Magnetron Sputtering of Hard and Optically Transparent HfO 2 Films. *Surface and Coatings Technology* **2016**, *290*, 58–64, doi:10.1016/j.surfcoat.2015.08.024.
8. Ristau, D.; Gross, T. Ion Beam Sputter Coatings for Laser Technology. In proceedings of the Optical Systems Design, Jena, Germany, September 30 2005; Amra, C., Kaiser, N., Macleod, H.A., Eds.; p. 596313, doi: 10.1117/12.624772.
9. Siegle, L.; Ristok, S.; Giessen, H. Complex Aspherical Singlet and Doublet Microoptics by Grayscale 3D Printing. *Opt. Express* **2023**, *31*, 4179, doi:10.1364/OE.480472.
10. Gonzalez-Hernandez, D.; Varapnickas, S.; Bertoncini, A.; Liberale, C.; Malinauskas, M. Micro-Optics 3D Printed via Multi-Photon Laser Lithography. *Advanced Optical Materials* **2023**, *11*, 2201701, doi:10.1002/adom.202201701.
11. Varapnickas, S.; Chandran Thodika, S.; Moroté, F.; Juodkazis, S.; Malinauskas, M.; Brasselet, E. Birefringent Optical Retarders from Laser 3D-Printed Dielectric Metasurfaces. *Applied Physics Letters* **2021**, *118*, 151104, doi:10.1063/5.0046978.
12. Grinevičiūtė, L. Nanostructured Optical Coatings for the Manipulation of Laser Radiation. PhD, Vilnius University: Lithuania, 2021.
13. Pfeiffer, K.; Schulz, U.; Tünnermann, A.; Szeghalmi, A. Antireflection Coatings for Strongly Curved Glass Lenses by Atomic Layer Deposition. *Coatings* **2017**, *7*, 118, doi:10.3390/coatings7080118.

14. Paul, P.; Pfeiffer, K.; Szeghalmi, A. Antireflection Coating on PMMA Substrates by Atomic Layer Deposition. *Coatings* **2020**, *10*, 64, doi:10.3390/coatings10010064.
15. Ristok, S.; Flad, P.; Giessen, H. Atomic Layer Deposition of Conformal Anti-Reflective Coatings on Complex 3D Printed Micro-Optical Systems. *Opt. Mater. Express* **2022**, *12*, 2063, doi:10.1364/OME.454475.
16. Arriaga Dávila, J.; Winczewski, J.P.; Herrera-Zaldívar, M.; Murillo-Bracamontes, E.A.; Rosero Arias, C.; Pineda-Aguilar, N.; Cholula-Díaz, J.L.; De Leon, I.; Gardeniers, H.; Susarrey Arce, A.; et al. Enabling High-Quality Transparent Conductive Oxide on 3D Printed ZrO2 Architectures through Atomic Layer Deposition. *Applied Surface Science* **2023**, *636*, 157796, doi:10.1016/j.apsusc.2023.157796.
17. George, S.M. Atomic Layer Deposition: An Overview. *Chem. Rev.* **2010**, *110*, 111–131, doi:10.1021/cr900056b.
18. Merkininkaitė, G.; Aleksandravičius, E.; Malinauskas, M.; Gailevičius, D.; Šakirzanovas, S. Laser Additive Manufacturing of Si/ZrO_2 Tunable Crystalline Phase 3D Nanostructures. *OEA* **2022**, *5*, 210077–210077, doi:10.29026/oea.2022.210077.
19. Gailevicius, D.; Zvirblis, R.; Galvanauskas, K.; Bataviciute, G.; Malinauskas, M. Calcination-Enhanced Laser-Induced Damage Threshold of 3D Micro-Optics Made with Laser Multi-Photon Lithography. *Photonics* **2023**, *10*, 597, doi:10.3390/photonics10050597.
20. Ovsianikov, A.; Viertl, J.; Chichkov, B.; Oubaha, M.; MacCraith, B.; Sakellari, I.; Giakoumaki, A.; Gray, D.; Vamvakaki, M.; Farsari, M.; et al. Ultra-Low Shrinkage Hybrid Photosensitive Material for Two-Photon Polymerization Microfabrication. *ACS Nano* **2008**, *2*, 2257–2262, doi:10.1021/nn800451w.
21. D. Gonzalez-Hernandez, B. Sanchez-Padilla, D. Gailevičius, S. Chandran Thodika, S. Juodkazis, E. Brasselet, M. Malinauskas, Single-step 3D printing of micro-optics with adjustable refractive index by ultrafast laser nanolithography, *Adv. Opt. Mater.* **2023**, doi:10.1002/adom.202300258.
22. The OptiLayer thin film software. Available online: https://optilayer.com/ (accessed on 8 July 2023).
23. Dudziak, M.; Topolniak, I.; Silbernagl, D.; Altmann, K.; Sturm, H. Long-Time Behavior of Surface Properties of Microstructures Fabricated by Multiphoton Lithography. *Nanomaterials* **2021**, *11*, 3285, doi:10.3390/nano11123285.
24. Bauer, J.; Izard, A.G.; Zhang, Y.; Baldacchini, T.; Valdevit, L. Thermal Post-Curing as an Efficient Strategy to Eliminate Process Parameter Sensitivity in the Mechanical Properties of Two-Photon Polymerized Materials. *Opt. Express* **2020**, *28*, 20362, doi:10.1364/OE.395986.
25. Lingnau, J.; Meyerhoff, G. The Spontaneous Polymerization of Methyl Methacrylate: 6. Polymerization in Solution: Participation of Transfer Agents in the Initiation Reaction. *Polymer* **1983**, *24*, 1473–1478, doi:10.1016/0032-3861(83)90233-1.
26. Femtika Ltd. Available online: https://femtika.com/ (accessed on 8 July 2023).
27. Jonušauskas, L.; Gailevičius, D.; Rekštytė, S.; Baldacchini, T.; Juodkazis, S.; Malinauskas, M. Mesoscale Laser 3D Printing. *Opt. Express* **2019**, *27*, 15205, doi:10.1364/OE.27.015205.
28. OpenSCAD software. Available online: https://openscad.org/ (accessed on 8 July 2023).
29. Skliutas, E.; Samsonas, D.; Čiburys, A.; Kontenis, L.; Gailevicius, D.; Narbutis, D.; Jukna, V.; Vengris, M.; Juodkazis, S.; Malinauskas, M. X-Photon Laser Direct Write 3D Nanolithography, *Virtual and Physical Prototyping* **2023**, 18:1, doi: 10.1080/17452759.2023.2228324.
30. Janssen, G.C.A.M.; Abdalla, M.M.; Van Keulen, F.; Pujada, B.R.; Van Venrooy, B. Celebrating the 100th Anniversary of the Stoney Equation for Film Stress: Developments from Polycrystalline Steel Strips to Single Crystal Silicon Wafers. *Thin Solid Films* **2009**, *517*, 1858–1867, doi:10.1016/j.tsf.2008.07.014.
31. Kwon, S.-H.; Kwon, O.-K.; Kim, J.-H.; Oh, H.-R.; Kim, K.-H.; Kang, S.-W. Initial Stages of Ruthenium Film Growth in Plasma-Enhanced Atomic Layer Deposition. *J. Electrochem. Soc.* **2008**, *155*, H296, doi:10.1149/1.2868779.
32. Wilson, C.A.; Grubbs, R.K.; George, S.M. Nucleation and Growth during Al_2O_3 Atomic Layer Deposition on Polymers. *Chem. Mater.* **2005**, *17*, 5625–5634, doi:10.1021/cm050704d.
33. Spagnola, J.C.; Gong, B.; Arvidson, S.A.; Jur, J.S.; Khan, S.A.; Parsons, G.N. Surface and Sub-Surface Reactions during Low Temperature Aluminium Oxide Atomic Layer Deposition on Fiber-Forming Polymers. *J. Mater. Chem.* **2010**, *20*, 4213, doi:10.1039/c0jm00355g.
34. Jur, J.S.; Spagnola, J.C.; Lee, K.; Gong, B.; Peng, Q.; Parsons, G.N. Temperature-Dependent Subsurface Growth during Atomic Layer Deposition on Polypropylene and Cellulose Fibers. *Langmuir* **2010**, *26*, 8239–8244, doi:10.1021/la904604z.
35. Puurunen, R.L.; Vandervorst, W. Island Growth as a Growth Mode in Atomic Layer Deposition: A Phenomenological Model. *Journal of Applied Physics* **2004**, *96*, 7686–7695, doi:10.1063/1.1810193.
36. Guo, H.C.; Ye, E.; Li, Z.; Han, M.-Y.; Loh, X.J. Recent Progress of Atomic Layer Deposition on Polymeric Materials. *Materials Science and Engineering: C* **2017**, *70*, 1182–1191, doi:10.1016/j.msec.2016.01.093.
37. Žukauskas, A.; Batavičiūtė, G.; Ščiuka, M.; Balevičius, Z.; Melninkaitis, A.; Malinauskas, M. Effect of the Photoinitiator Presence and Exposure Conditions on Laser-Induced Damage Threshold of ORMOSIL (SZ2080). *Optical Materials* **2015**, *39*, 224–231, doi:10.1016/j.optmat.2014.11.031.
38. Paul, P.; Beladiya, V.; Kästner, D.; Schulz, U.; Burkhardt, M.; Szeghalmi, A.V. Conformal Antireflection Coating on Polycarbonate Domes. In Proceedings of the Advances in Optical Thin Films VII; Lequime, M., Ristau, D., Eds.; SPIE: Online Only, Spain, September 12 2021; p. 11, doi: 10.1117/12.2595915 .
39. Design software for optical thin films. Available online: https://www.hulinks.co.jp/en (accessed on 8 July 2023).
40. Lau, W.S.; Zhang, J.; Wan, X.; Luo, J.K.; Xu, Y.; Wong, H. Surface Smoothing Effect of an Amorphous Thin Film Deposited by Atomic Layer Deposition on a Surface with Nano-Sized Roughness. *AIP Advances* **2014**, *4*, 027120, doi:10.1063/1.4866988.

41. Elam, J.W.; Sechrist, Z.A.; George, S.M. ZnOyAl2O3 Nanolaminates Fabricated by Atomic Layer Deposition: Growth and Surface Roughness Measurements. *Thin Solid Films* **2002**, 414, 43-55, doi: 10.1016/S0040-6090(02)00427-3.
42. Myers, T.J.; Throckmorton, J.A.; Borrelli, R.A.; O'Sullivan, M.; Hatwar, T.; George, S.M. Smoothing Surface Roughness Using Al2O3 Atomic Layer Deposition. *Applied Surface Science* **2021**, *569*, 150878, doi:10.1016/j.apsusc.2021.150878.
43. Fang, M.; Li, J.; He, H.; Fan, Z.; Xiao, Q.; Li, Z. Evolution and Control of Optical Thin Film Stress.; Yang, L., Ruch, E., Li, S., Eds.; Xiamen, China, October 16 2012; p. 84160K, doi:10.1117/12.2009292.
44. Liu, H.; Jensen, L.; Ma, P.; Ristau, D. Stress Compensated Anti-Reflection Coating for High Power Laser Deposited with IBS SiO2 and ALD Al2O3. *Applied Surface Science* **2019**, *476*, 521–527, doi:10.1016/j.apsusc.2019.01.125.